AIAA JOURNAL
Vol. 48, No. 12, December 2010

Least-Squares Continuous Sensitivity Shape Optimization for Structural Elasticity Applications

Douglas P. Wickert*
Air Force Institute of Technology, Wright-Patterson Air Force Base, Ohio 45433-7765
Robert A. Canfield†
Virginia Polytechnic Institute and State University, Blacksburg, Virginia 24061
and
J. N. Reddy‡
Texas A&M University, College Station, Texas 77843-3123

DOI: 10.2514/1.44349

A general first-order formulation of the continuous sensitivity equations is introduced that improves the accuracy of the sensitivity boundary conditions. In the continuous sensitivity method, design or shape parameter gradients are computed from a continuous system of partial differential equations instead of the discretized system, which avoids the problematic mesh sensitivity calculations of discrete methods for shape variation problems. The first-order formulation for both the underlying elasticity and sensitivity equations is amenable to solution by a high-order polynomial least-squares finite element model. The continuous sensitivity boundary-value problem, which can be posed in local or total derivative form, is generally simpler in local sensitivity form for shape variation problems. Although the local form is not unique and total material sensitivities are generally desired for structural elasticity problems, the local sensitivity solution is easily transformed to a material derivative. The first-order formulation and the transformation to material derivatives are demonstrated for two elasticity example problems. The least-squares continuous sensitivity solutions are presented and compared with analytic sensitivities and finite difference results and should prove convenient validation benchmarks for other continuous sensitivity applications.

I. Introduction

DESIGN sensitivity methods can be grouped into numerical approximate methods (e.g., finite difference) and analytic and semianalytic methods. Analytic and semianalytic methods can be further classified as either discrete or continuous, the difference depending on the order of the discretization and differentiation steps [1,2]. The most common approach is to discretize the system first and then calculate sensitivities by either direct or adjoint methods. For shape sensitivity problems, the boundary and domain of the problem vary with the design parameters, and the mesh sensitivity must be calculated in the discrete approach. In the continuous sensitivity method, also known as variational shape design [1], the continuum sensitivity method [3], and the variational sensitivity method [4], the design parameter gradients are calculated by solving the continuous sensitivity equations (CSEs), typically a system of partial differential equations [5]. Since the CSE system is posed as a continuous system, it can efficiently produce shape parameter gradients without calculating the mesh sensitivity (which often amounts to the expensive task of inverting a large mesh Jacobian). Furthermore, the sensitivity system is always a linear system of equations, even when the original system is nonlinear.

Continuous sensitivity methods were first introduced for structural problems [3,6], but few applications to structural problems appear in the literature. The landmark paper of Borggaard and Burns [7] introduced the CSE nomenclature in a fluid setting, and several fluid flow optimization applications followed [5,8–10]. Although there now exists an extensive body of literature describing and documenting the application of continuous sensitivity methods to fluid dynamics problems, the applications to nonfluid problems have largely been limited to one-dimensional scalar problems (e.g., heat flow) and one-dimensional beam problems [10]. Bhaskaran and Berkooz [8] present a finite-element-method-based continuous sensitivity solution for a two-dimensional structural elasticity problem that is also considered in this paper, but much of the useful detail and validation of the gradient information of the solution was not included. More recently, Étienne and Pelletier [11] and Étienne et al. [12,13] have employed sensitivity methods for a range of fluid–structure interaction problems, but there remains a dearth of structural elasticity applications that employ continuous sensitivity methods.

Continuous adjoint sensitivity methods also exist [14,15]. For problems with many design variables, load conditions, and few active constraints, the adjoint method is generally a more efficient means to obtain the desired sensitivities than direct sensitivity methods. An adjoint CSE method is also derived in [16]. Note that the adjoint sensitivity method can efficiently deliver the objective and constraint function sensitivities, but the sensitivity variables are not calculated as in the direct CSE method.

For shape variation problems, continuous sensitivity systems are typically posed in terms of local derivatives, although it is possible to derive the CSE system in total derivative form (Lagrangian description [17]). The local sensitivity is defined as the component of the total shape parameter derivative at a particular point in an Eulerian reference frame. The total sensitivity consists of the local derivative at a point in Eulerian space plus the transport effect of the shape variation as a material point moves as a function of the shape parameter. The CSEs are generally simpler to pose and solve in local-derivative form than in the total derivative form. For example, the total derivative form of the stress sensitivity derived in [3] requires an

Presented as Paper 2008-1797 at the 49th AIAA/ASME/ASCE/AHS/ASC Structures, Structural Dynamics, and Materials Conference; 16th AIAA/ASME/AHS Adaptive Structures Conference, Schaumburg, IL, 7–10 April 2008; received 13 March 2009; revision received 27 September 2009; accepted for publication 19 October 2009.

*Department of Aeronautical and Astronautical Engineering, 2950 Hobson Way. Member AIAA.
†Professor, Department of Aerospace and Ocean Engineering, 214 Randolph Hall. Associate Fellow AIAA.
‡Distinguished Professor, Department of Mechanical Engineering; jnreddy@tamu.edu. Fellow AIAA.

additional initial strain field for the sensitivity problem that is not part of the original elasticity problem. The local form for the stress sensitivity, also presented in [3], is more convenient; however, it depends on a domain transformation function that is not unique. Furthermore, for structural optimization problems, the design sensitivity at a material point is usually required, which necessitates a means to convert the local sensitivities from the CSE solution to total sensitivities at a given material point. Although the local sensitivity solution is not unique for shape variation problems, the total sensitivity obtained by converting the local derivative to the total derivative at a material point is unique.

The solutions described next employ the least-squares finite element model (LSFEM) for both the CSE problem and the original structural problem from which the CSE boundary conditions are derived. The choice of LSFEM is partially motivated by the fact that boundary gradients are used to establish boundary conditions for the CSE system, and first-order (mixed) formulations tend to produce better solution gradients for secondary (stress) responses than the traditional weak-form Galerkin approach [18]. Previous CSE applications [5,7,9–13] highlight the loss of accuracy for second-order boundary derivatives that arise from the Neumann-type boundary conditions of the original problem. In a first-order formulation of the underlying problem, however, only first-order boundary gradients appear in the sensitivity boundary conditions. A first-order least-squares (LS) formulation is also attractive for structural problems with mixed boundary conditions (e.g., both displacement and stress boundary conditions), because the element formulation is inherently mixed but without the usual stability problems associated with mixed Galerkin finite element models.

This paper begins with a general derivation of the first-order continuous sensitivity system and its associated boundary conditions. This is followed by a brief description of the LSFEM computational approach used to solve both the elasticity system and the CSE system. A one-dimensional bar example is used to illustrate the nonuniqueness of the local sensitivity form and the conversion from the local CSE solution to a total, material derivative. A classic elasticity problem of an unstressed hole in a plate is then introduced, solved, and compared with both a finite difference solution and a closed-form analytic solution. The objective is to provide sufficient detail in the derivation and results of the example problem so that the problem can serve as a verification benchmark for structural sensitivity analysis. The CSE design gradients are then employed in an optimization example.

II. Continuous Sensitivity Equations

A first-order formulation of the CSEs can reduce the loss of accuracy associated with Neumann-type boundary conditions, identified in [5,7,9–13]. In a first-order (mixed) formulation, derivatives of the solution on traditional Neumann boundaries are available as primal variables and can be enforced in the same manner as the Dirichlet boundary conditions. Thus, only first-order gradients are needed for the sensitivity boundary conditions when the original and sensitivity problems are posed in first-order form. First-order forms for elasticity have proven problematic for traditional FEM elasticity formulations [19–21] due to the min–max nature of the formulation and the requirement to satisfy the Ladyzhenskaya–Babuška–Brezzi (LBB) condition [22]. This can be avoided by using a LSFEM formulation [23] and is considered in Sec. IV.

Consider a general, nonlinear boundary-value system defined in a domain Ω with a boundary Γ for which we seek a solution $\mathbf{u}$ of the equations

$$\mathbf{A}(\mathbf{u})\mathbf{u} = \mathbf{f} \quad \text{in } \Omega \tag{1}$$

$$\mathbf{B}(\mathbf{u})\mathbf{u} = \mathbf{g} \quad \text{on } \Gamma \tag{2}$$

where $\mathbf{A}(\mathbf{u})$ is a first-order time-space nonlinear differential operator defined by

$$\mathbf{A} \equiv \mathbf{A}_t \frac{\partial}{\partial t} + \sum_{i=1}^{\dim} \mathbf{A}_i \frac{\partial}{\partial x_i} + \mathbf{A}_0 \tag{3}$$

and where $\mathbf{A}_t$, $\mathbf{A}_i$, and $\mathbf{A}_0$ are the component matrices and $\mathbf{u} = \{u_1, u_2, \ldots, u_n\}^T$. The system is nonlinear if the operator, $\mathbf{A}$ or $\mathbf{B}$, is a function of the solution $\mathbf{u}$. The boundary operator $\mathbf{B}(\mathbf{u})$ is similarly defined:

$$\mathbf{B} = \mathbf{B}_t \frac{\partial}{\partial t} + \sum_{i=1}^{\dim -1} \mathbf{B}_i \frac{\partial}{\partial \xi_i} + \mathbf{B}_0 \tag{4}$$

In Eq. (4), ξ_i denotes the coordinates that parameterize the boundary, which are naturally at least one dimension less than the domain dimension.

In the CSE method, the sensitivity of $\mathbf{u}$ to a design parameter is the solution to the sensitivity equations obtained by differentiating the system in Eqs. (1) and (2) with respect the design parameter. Thus, differentiating Eq. (1) with respect to a design parameter b,

$$\tfrac{\partial}{\partial b}[\mathbf{A}_0(\mathbf{u};b)\mathbf{u} + \mathbf{A}_i(\mathbf{u};b)\mathbf{u}_{,i} + \mathbf{A}_t(\mathbf{u};b)\mathbf{u}_{,t}] = \tfrac{\partial}{\partial b}[\mathbf{f}(\mathbf{x};b)] \tag{5}$$

is used to form the first-order CSEs. Partial differentiation is denoted by the subscripted comma notation in Eq. (5) that, in component form, is

$$\tfrac{\partial}{\partial b}[a_{ij}^{(0)}(\mathbf{u};b)u_j + a_{ij}^{(k)}(\mathbf{u};b)u_{j,k} + a_{ij}^{(t)}(\mathbf{u};b)u_{j,t}] = \tfrac{\partial}{\partial b}[f_i(\mathbf{x};b)] \tag{6}$$

where the parenthetical superscript is used to denote the operator and the index k ranges from one up to the domain dimension. Equation (6) expands as

$$\begin{aligned}&\left[\frac{\partial a_{ij}^{(0)}}{\partial b}u_j + \frac{\partial a_{ij}^{(0)}}{\partial u_m}\frac{\partial u_m}{\partial b}u_j + a_{ij}^{(0)}\frac{\partial u_j}{\partial b}\right]\\ &\quad + \left[\frac{\partial a_{ij}^{(k)}}{\partial b}u_{j,k} + \frac{\partial a_{ij}^{(k)}}{\partial u_m}\frac{\partial u_m}{\partial b}u_{j,k} + a_{ij}^{(k)}\frac{\partial u_{j,k}}{\partial b}\right] + \frac{\partial a_{ij}^{(t)}}{\partial b}u_{j,t}\\ &\quad + \frac{\partial a_{ij}^{(t)}}{\partial u_m}\frac{\partial u_m}{\partial b}u_{j,t} + a_{ij}^{(t)}\frac{\partial u_{j,t}}{\partial b} = \frac{\partial}{\partial b}f_i(\mathbf{x};b)\end{aligned} \tag{7}$$

Since the spatial-temporal derivatives are independent operations from the sensitivity derivative, the order of differentiation may be reversed. Note that this commutation of differentiation is not possible if the sensitivity derivative in Eq. (5) is not a local derivative [1]. The $\partial u_m/\partial b$ terms are referred to as the sensitivity variables; they represent how the solution changes with respect to a design parameter. Collecting the sensitivity variables in Eq. (7) then yields the continuous sensitivity system:

$$\begin{aligned}&\left[a_{im}^{(0)} + \frac{\partial a_{ij}^{(0)}}{\partial u_m}u_j + \frac{\partial a_{ij}^{(k)}}{\partial u_m}u_{j,k} + \frac{\partial a_{ij}^{(t)}}{\partial u_m}u_{j,t}\right]\frac{\partial u_m}{\partial b}\\ &\quad + [a_{im}^{(k)}]\frac{\partial u_{m,k}}{\partial b} + [a_{im}^{(t)}]\frac{\partial u_{m,t}}{\partial b}\\ &\quad = \frac{\partial}{\partial b}f_i(\mathbf{x};b) - \left[u_j\frac{\partial a_{ij}^{(0)}}{\partial b} + u_{j,k}\frac{\partial a_{ij}^{(k)}}{\partial b} + u_{j,t}\frac{\partial a_{ij}^{(t)}}{\partial b}\right]\end{aligned} \tag{8}$$

Defining the components of the ${}^b\mathbf{A}_0$ sensitivity matrix by

$${}^b a_{ij}^{(0)} = a_{ij}^{(0)} + \frac{\partial a_{il}^{(0)}}{\partial u_j}u_l + \frac{\partial a_{il}^{(k)}}{\partial u_j}u_{l,k} + \frac{\partial a_{il}^{(t)}}{\partial u_j}u_{l,t} \tag{9}$$

yields the first-order matrix differential-operator form of the sensitivity equations:

$$\begin{aligned}&[{}^b\mathbf{A}_0]({}^b\mathbf{u}) + [\mathbf{A}_i]({}^b\mathbf{u})_{,i} + [\mathbf{A}_t]({}^b\mathbf{u})_{,t}\\ &\quad = \mathbf{f}_{,b}(\mathbf{x};b) - [\mathbf{A}_{0,b}\mathbf{u} + \mathbf{A}_{i,b}\mathbf{u}_{,i} + \mathbf{A}_{t,b}\mathbf{u}_{,t}]\end{aligned} \tag{10}$$

where ${}^b\mathbf{u} \equiv \mathbf{u}_{,b}$ is used to denote the sensitivity variable. In the examples that follow, the superscript prefix notation ${}^b\mathbf{u}$, representing

the solution to the CSEs, will be treated as distinct from the analytic sensitivity. The analytic sensitivity, denoted by $\mathbf{u}_{,b}$ next, is the sensitivity determined by taking the derivative of an analytic solution $\mathbf{u}$ of the system in Eqs. (1) and (2) with respect to the design parameter b.

The ${}^{b}\mathbf{A}_0$ sensitivity matrix, defined in component form by Eq. (9), may also be expressed in matrix form as

$$\begin{aligned}{}^{b}\mathbf{A}_0 &= \mathbf{A}_0 + \mathbf{A}_{0,u_1}[\{\mathbf{u}\}\{0\}\cdots\{0\}] + \mathbf{A}_{0,u_2}[\{0\}\{\mathbf{u}\}\cdots\{0\}] \\ &\quad + \mathbf{A}_{0,u_n}[\{0\}\ldots\cdots\{0\}\{\mathbf{u}\}] + \cdots + \mathbf{A}_{1,u_1}[\{\mathbf{u}_{,x_1}\}\{0\}\cdots\{0\}] \\ &\quad + \mathbf{A}_{1,u_2}[\{0\}\{\mathbf{u}_{,x_1}\}\cdots\{0\}] + \mathbf{A}_{1,u_n}[\{0\}\cdots\{0\}\{\mathbf{u}_{,x_1}\}] + \cdots \\ &\quad + \mathbf{A}_{t,u_1}[\{\mathbf{u}_{,t}\}\{0\}\cdots\{0\}] + \mathbf{A}_{t,u_2}[\{0\}\{\mathbf{u}_{,t}\}\cdots\{0\}] \\ &\quad + \mathbf{A}_{t,u_n}[\{0\}\cdots\{0\}\{\mathbf{u}_{,t}\}] \end{aligned} \tag{11}$$

or more compactly as

$${}^{b}\mathbf{A}_0 = \mathbf{A}_0 + \frac{\partial \mathbf{A}_0}{\partial u_i}[u_i\delta_{ji}] + \frac{\partial \mathbf{A}_k}{\partial u_i}[u_{i,k}\delta_{ji}] + \frac{\partial \mathbf{A}_t}{\partial u_i}[u_{i,t}\delta_{ji}] \tag{12}$$

Note that the gradient operators, $\mathbf{A}_i$ in Eq. (3), are unchanged for the CSE system [Eq. (10)]. Furthermore, for linear systems, the sensitivity matrix ${}^{b}\mathbf{A}_0 = \mathbf{A}_0$. Equation (8) includes both the explicit dependence of the system solution on b (e.g., as with sizing or shape sensitivity), as well as the implicit nonlinear dependence of the system solution on b (e.g., as in shape optimization). Additionally, in shape sensitivity problems, where b represents a boundary shape parameter, the system operators typically have no explicit dependence on b, and the bracketed terms on the right-hand side of Eq. (10) (e.g., $\mathbf{A}_{i,b}$) vanish. Thus, for linear, shape variation problems, the component CSE operators are identical to the original system operators, and the CSEs and original systems are the same except for the boundary conditions.

The continuous sensitivity system in Eq. (10) is always linear in the sensitivity variable $\mathbf{u}_{,b}$. The conclusion that only the ${}^{b}\mathbf{A}_0$ operator changes from the original system for a nonlinear system is due to the first-order form and the result that the original system is only nonlinear in $\mathbf{u}$. When the original parent system is written in first-order form, the nonlinear terms can always be factored as $\mathbf{A}(\mathbf{u})\mathbf{u}$, so that the nonlinearities appear explicitly in vector $\mathbf{u}$.

The CSE boundary operator system can be derived from Eq. (2) in the same manner. Thus,

$$\begin{aligned}&\left[\mathbf{B}_0 + \frac{\partial \mathbf{B}_0}{\partial u_i}[\{u_i\}\delta_{ji}] + \frac{\partial \mathbf{B}_\xi}{\partial u_i}[\{u_{i,\xi}\}\delta_{ji}]\right]{}^{b}\mathbf{u} + \mathbf{B}_\xi\,{}^{b}\mathbf{u}_{,\xi} \\ &\quad = \mathbf{g}_{,b}(\mathbf{x};b) - [\mathbf{B}_{0,b}\mathbf{u} + \mathbf{B}_{\xi,b}\mathbf{u}_{,\xi}] \quad \text{on } \Gamma\end{aligned} \tag{13}$$

Both Eqs. (10) and (13) were derived using local derivatives. Equation (13) is valid for nonshape problems and for shape problems in which a particular boundary is not a function of the shape parameter. For shape variation problems that also change the boundary location, the material points $\mathbf{X}$ that define the boundary Γ (Lagrangian description) are a function of the design parameter b. Thus, evaluation of Eq. (13), which is derived in terms of the Eulerian points $\mathbf{x}$, must account for the total variation of the boundary. The local and total (material) derivatives are related by

$$\mathrm{D}_b(\mathbf{u}) \equiv \left.\frac{\mathrm{D}\mathbf{u}}{\mathrm{D}b}\right|_{\mathbf{X}} = \left.\frac{\partial \mathbf{u}}{\partial b}\right|_{\mathbf{x}} + \nabla\mathbf{u}\cdot\left.\frac{\partial \mathbf{X}_\Omega}{\partial b}\right|_{\mathbf{X}} \tag{14}$$

where $\mathrm{D}_b(\cdot)$ is the material derivative operator with respect to the parameter b. Note that the gradient operation and dot product in the transport term are carried out componentwise. Thus, the total derivative of $\mathbf{u}$ with respect to b at a material point $\mathbf{X}$ consists of the local derivative of $\mathbf{u}$ with respect to parameter b and the convective transport term, which accounts for how the material point $\mathbf{X}$ moves as the design parameter b varies. Solving Eq. (14) for the local derivative gives the desired sensitivity variable boundary condition for the CSE system in local-derivative form:

$${}^{b}\mathbf{u}|_\Gamma \equiv \left.\frac{\partial \mathbf{u}}{\partial b}\right|_{\mathbf{X}=\Gamma} = \left.\frac{\mathrm{D}\mathbf{u}}{\mathrm{D}b}\right|_\Gamma - \nabla\mathbf{u}\cdot\frac{\partial \mathbf{X}_{\Gamma(b)}}{\partial b} \tag{15}$$

where in two dimensions

$$\mathbf{X}_{\Gamma(b)} = \{(x,y) \in \Gamma(b)\} \tag{16}$$

are coordinates (ordered pairs in $\mathbf{R}^2$) that define the boundary as a function of b. The first term on the right side of Eq. (15) accounts for how the boundary conditions for the problem change with respect to the design parameter. In most cases, this term is zero. That is, the boundary condition often does not change as the shape changes. The convection term is the dot product of the derivative of the set of spatial coordinates that define the boundary with the gradient of the solution to Eq. (1), where for vectors, the gradient operation is carried out row-wise. In the examples considered next, the gradient in the convection term is calculated by taking derivatives of the finite element approximation shape functions.

Compare the form in Eq. (15) to the classic continuum stress sensitivity expression derived by Dems and Haftka [3] (valid both on the boundary and throughout the domain),

$${}^{b}\sigma_{ij}n_j = \frac{\mathrm{D}T_i}{\mathrm{D}b} - \sigma_{ij,k}n_j\frac{\partial \phi_k}{\partial b} - \sigma_{ij}(n_jn_l - \delta_{jl})n_k\left[\frac{\partial \phi_k}{\partial b}\right]_{,l} \tag{17}$$

where T_i are the components of the surface traction vector, n_i are the components of the unit normal vector, δ is the Kronecker delta function, and ϕ is the transformation field that maps material coordinates of the domain as a function of the design parameter. We now show that Eq. (17) is equivalent to Eq. (15) when $\mathbf{u} = \{\sigma_n \quad \sigma_\tau\}^T$, and the former is expressed in coordinates normal and tangential to the boundary surface. The stress vector is [22,24]

$$\begin{Bmatrix}\sigma_n \\ \sigma_\tau\end{Bmatrix} \equiv [\underline{\sigma}]^T\cdot\{\hat{\mathbf{n}}\} = \mathbf{T}^{(\hat{\mathbf{n}})} = \begin{Bmatrix}T_n \\ T_s\end{Bmatrix} \tag{18}$$

where σ_n and σ_τ are the normal and shear components of the stress vector. At any point in the normal-tangential coordinate reference frame on the boundary, we have $n_1 = 1$ and $n_2 = 0$. For the normal stress component, $\sigma_n = \sigma_{11}n_1$ and $(n_1n_l - \delta_{1l}) = 0$, so that the final term in Eq. (17) vanishes when it is also expressed in the normal-tangential coordinate reference frame. Similarly, for the tangential shear stress component, $\sigma_\tau = \sigma_{21}n_1$ and $(n_1n_l - \delta_{1l}) = 0$, so that the final term in Eq. (17) again vanishes. Thus, the evaluation of Eq. (17) in the normal-tangential coordinate system yields

$$\begin{aligned}\begin{Bmatrix}{}^{b}\sigma_n \\ {}^{b}\sigma_\tau\end{Bmatrix} &= \begin{Bmatrix}{}^{b}\sigma_{11} \\ {}^{b}\sigma_{21}\end{Bmatrix} = \frac{\mathrm{D}}{\mathrm{D}b}\begin{Bmatrix}T_1 \\ T_2\end{Bmatrix} \\ &\quad - \begin{Bmatrix}\sigma_{11,1}n_1\cdot\phi_{1,b} + \sigma_{11,2}n_1\cdot\phi_{2,b} \\ \sigma_{21,1}n_1\cdot\phi_{1,b} + \sigma_{21,2}n_1\cdot\phi_{2,b}\end{Bmatrix}_{\Gamma(b)} \\ &= \frac{\mathrm{D}\mathbf{T}^{(\hat{\mathbf{n}})}}{\mathrm{D}b} - \nabla\begin{Bmatrix}\sigma_n \\ \sigma_\tau\end{Bmatrix}\cdot\mathbf{X}_{,b}\end{aligned} \tag{19}$$

Not surprisingly, the stress tensor sensitivity is simplified by expressing it in a normal-tangential coordinate system, which permits a vector expression and the use of Eq. (15). Furthermore, Eq. (15) is valid for any vector field quantity; our primary interest for elasticity applications will be deformation and stress. Note that, in both Eqs. (15) and (17), the choice of boundary parameterization $\mathbf{X}_{\Gamma(b)}$ or transformation function ϕ, respectively, is not unique. Thus, the solution to the local-derivative form of the CSEs is also not unique. This is demonstrated in a straightforward example in the next section.

III. Nonuniqueness of Local Derivatives

The CSE system [Eqs. (10) and (13)] was derived and posed in terms of local derivatives. For shape variation problems, the local-derivative sensitivity boundary conditions depend on the boundary

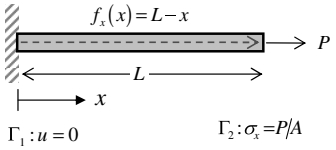

Fig. 1 Elastic bar example.

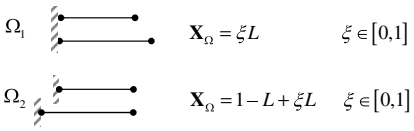

Fig. 2 Two possible domain parameterizations for bar length.

parameterization or domain transformation function and are not unique. This is demonstrated in an example. Consider the one-dimensional elastic structure (bar) depicted in Fig. 1. The first-order field equations governing the stress and displacement are

$$(A\sigma_x)_{,x} + f_x = 0 \tag{20}$$

$$Eu_{,x} - \sigma_x = 0 \tag{21}$$

where u is the axial displacement, σ_x is the axial stress, A is the cross-sectional area of the bar, f_x is the applied axial force, and E is Young's modulus. Equations (20) and (21) may be directly integrated to yield the analytic stress and displacement solutions that, for constant a cross-sectional area, yield

$$\sigma_x(x; L) = \frac{x^2}{2A} - \frac{Lx}{A} + \frac{L^2}{2A} + \frac{P}{A} \tag{22}$$

$$u(x; L) = \frac{x^3}{6EA} - \frac{Lx^2}{2EA} + \frac{L^2 x}{2EA} + \frac{Px}{EA} \tag{23}$$

Taking bar length as a shape parameter, we will explore two natural parameterizations of the bar to demonstrate the nonuniqueness of the local CSE solution. In the first depicted, in Fig. 2, the domain is parameterized by L so that material points at the tip of the bar move to the right in Eulerian space as the beam length increases. In the second parameterization, material points at the base of the bar move to the left in Eulerian space, while the tip of the bar remains fixed in space. Since this is a linear system, the bar-length CSEs are identical to the elasticity field equations (20) and (21), except that the sensitivity variables replace the stress and displacement variables, and the body force is replaced by the body force sensitivity. Thus, for a constant cross-sectional area, the CSE system is

$$^L\sigma_{x,x} + \tfrac{1L}{A} f_x = 0 \tag{24}$$

$$^L u_{,x} - \tfrac{1L}{E}\sigma_x = 0 \tag{25}$$

Although the CSEs have the same form as the field equations (20) and (21), the sensitivity boundary conditions depend on the boundary parameterization through Eq. (15). The sensitivity boundary data, body force, and local CSE solutions for this example are summarized in Table 1. The local CSE solution is obtained by integrating Eqs. (24) and (25) with the boundary data in Table 1. The results for both domain parameterizations are plotted in Fig. 3.

The local sensitivities are converted to total sensitivities by Eq. (14) using the appropriate domain sensitivity expression from Table 1. Thus, for the first parameterization, the total derivative displacement sensitivity is

$$\begin{aligned} \mathrm{D}_L(u)_{\Omega_1} &= {}^L u + \nabla u \cdot \mathbf{X}_{\Omega,L} \\ &= \frac{Lx}{AE} - \frac{x^2}{2AE} + \left(\frac{x^2}{2EA} - \frac{Lx}{AE} + \frac{L^2}{2EA}\right)(x) \end{aligned} \tag{26}$$

where ∇u is easily obtained from Eq. (23). For the second parameterization, the total displacement sensitivity is

$$\mathrm{D}_L u(x)_{\Omega_2} = \frac{L^2}{2EA} + \left(\frac{x^2}{2EA} - \frac{Lx}{AE} + \frac{L^2}{2EA}\right)(x-1) = \mathrm{D}_L u(x)_{\Omega_1} \tag{27}$$

which matches the total derivative sensitivity for the first parameterization. As implied by the dependence on the nonunique boundary parameterization in Eq. (15) and, equivalently, the free choice of the transformation field in Eq. (17), local sensitivities are not unique. However, the total derivatives, which are given at material coordinates, are unique. Structural optimization problems typically require the design sensitivity at a material point. Thus, optimization for structures should usually be based on gradients determined from total derivatives. The CSE problem is generally simpler to pose and solve in terms of local sensitivities due to the commutative property of local derivatives, as observed in Sec. II. Equation (14), however, gives a straightforward means to convert the local-derivative CSE solution to the total sensitivities for optimization.

The total derivative stress sensitivity for the bar example is obtained in the same manner as displacement.

$$\mathrm{D}_L\sigma(x)_{\Omega_1} = {}^L\sigma + \nabla\sigma \cdot \mathbf{X}_{\Omega,L} = \frac{L}{A} - \frac{x}{A} + \left(\frac{x}{A} - \frac{L}{A}\right)(x) \tag{28}$$

$$\mathrm{D}_L\sigma(x)_{\Omega_2} = 0 + \left(\frac{x}{A} - \frac{L}{A}\right)(x-1) = \mathrm{D}_L\sigma(x)_{\Omega_1} \tag{29}$$

The local CSE solution and the transport term for the two parameterizations in Fig. 1 are plotted with the total derivative CSE solution for stress and displacement in Fig. 3. As expected, the total derivative sensitivity matches the finite difference sensitivity solution, since finite difference results are, by nature, approximations to total derivatives. The finite difference solution is calculated by the first-forward finite difference:

$$\Delta_L(\mathbf{u}) = \frac{\mathbf{u}(L + \delta L) - \mathbf{u}(L)}{\delta L} \tag{30}$$

for a step size of $\delta L/L = 10^{-8}$.

In this example, the sensitivity equations could be directly integrated to give an analytic solution to the CSE system. For more

Table 1 Bar CSE boundary data, body force, and local solution

Parameterization	Ω_1	Ω_2
Boundary parameterization	$\mathbf{X}_{\Gamma_1} = \{0\}$, $\mathbf{X}_{\Gamma_2} = \{L\}$	$\mathbf{X}_{\Gamma_1} = \{1-L\}$, $\mathbf{X}_{\Gamma_2} = \{1\}$
Domain sensitivity	$\mathbf{X}_{\Omega,L} = \xi$	$\mathbf{X}_{\Omega,L} = \xi - 1$
Boundary data	$^L u(0) = 0$	$^L u(0) = -\nabla u \cdot \mathbf{X}_{,L}$
	$^L\sigma_x(L) = -\nabla\sigma_x \cdot \mathbf{X}_{,L} = -0 \cdot 1 = 0$	$= -(L^2/2EA)(-1) = L^2/2EA$
		$^L\sigma_x(L) = 0$
Body force sensitivity	$^L f_x = 1$	$^L f_x = 0$
Local CSE solution	$^L u(x) = Lx/AE - x^2/2AE$	$^L u(x) = L^2/2EA$
	$^L\sigma_x(x) = L/A - x/A$	$^L\sigma_x(x) = 0$

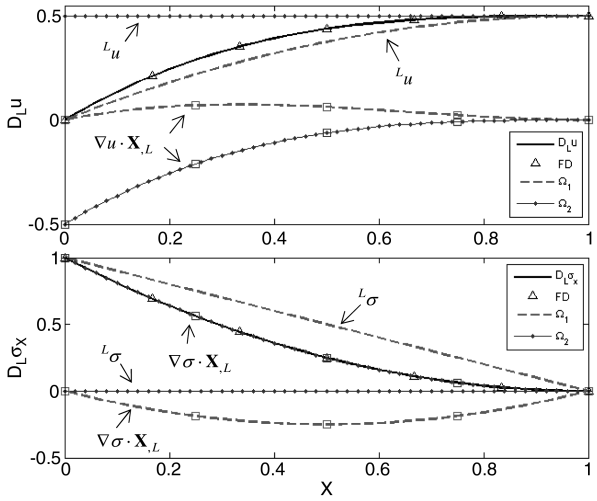

Fig. 3 Bar sensitivity comparison.

complex geometries and systems, a numerical solution (e.g., finite elements) is necessary to solve the sensitivity equations, but the initial steps are the same. It is usually possible to parameterize the domain in such a way that the material derivative vanishes on a boundary, so that the sensitivity boundary conditions are determined solely by the convection term in Eq. (15). The solution to the original system is used to generate the first term in the convective part of the sensitivity boundary conditions in Eq. (15). It is possible to pose the CSE system in terms of the total derivative (an example for the total derivative stress tensor sensitivity appears in [3]); however, it is usually more convenient to solve for the local sensitivity and then convert it to a material derivative through Eq. (14). The reason is that, although the conversion to the material derivative requires the transformation function ϕ for the entire domain when sensitivities are desired throughout the domain, it is not required for the solution of the CSE problem in local form. That is, only the parameterization or transformation of the boundary is necessary to pose the local CSEs for a shape variation problem. This not only simplifies the definition of the CSE problem, but it is alone sufficient if the optimization problem only requires the shape sensitivity on the boundary.

IV. Least-Squares Finite Element Model

In CSEs for elasticity, a first-order formulation for the elasticity equations is advantageous for the improved accuracy of the sensitivity boundary conditions. A first-order formulation of the CSEs eliminates the loss of accuracy associated with approximations for the higher-order gradients of the boundary solution, since only first-order gradients are needed for the sensitivity boundary conditions. However, a first-order formulation produces mixed elements, which have proven problematic for traditional FEM elasticity formulations without specially designed elements [19–21]. A LSFEM avoids the problem of satisfying the LBB condition [23] for mixed elements, because the LS functional is convex and is a natural choice for the solution of a first-order elasticity formulation.

The LSFEM model is based on the idea of minimization of the norm of the residual (or error) in the governing differential equations due to the approximation of the variables in the equations. The weighted sum of the squares of the system residuals defines the LS functional

$$J(\mathbf{u};\mathbf{f},\mathbf{g}) = \|\mathbf{A}\mathbf{u}-\mathbf{f}\|_\Omega^2 + \alpha_\Gamma \|\mathbf{B}\mathbf{u}-\mathbf{g}\|_\Gamma^2 \tag{31}$$

where α_Γ is a weighting parameter for the residual error in the boundary condition relative to the residual of the governing differential equation (both expressed in terms of the L^2 norm). Equation (31) represents a weak enforcement (i.e., integral sense) of the boundary conditions. The boundary conditions could alternatively be imposed directly on the boundary degrees of freedom (strong enforcement of the boundary conditions). A necessary condition for $\mathbf{u}$ to minimize Eq. (31) is that the first variation in Eq. (31) vanishes at $\mathbf{u}$. This yields an equivalent bilinear–linear inner product form [24] for the boundary-value system in Eqs. (1) and (2):

$$B(\mathbf{u},\mathbf{v}) = l(\mathbf{f},\mathbf{v}) \quad \forall\ \mathbf{v}\in\mathbf{V} \tag{32}$$

where the bilinear–linear inner product form for the domain is

$$B_\Omega(\mathbf{u},\mathbf{v}) \equiv (\mathbf{A}\mathbf{u},\mathbf{A}\mathbf{v}), \qquad l_\Omega(\mathbf{f},\mathbf{v}) \equiv (\mathbf{f},\mathbf{A}\mathbf{v}) \tag{33}$$

and the bilinear–linear inner product form for the boundary is

$$B_\Gamma(\mathbf{u},\mathbf{v}) \equiv (\mathbf{B}\mathbf{u},\mathbf{B}\mathbf{v}), \qquad l_\Gamma(\mathbf{g},\mathbf{v}) \equiv (\mathbf{g},\mathbf{B}\mathbf{v}) \tag{34}$$

The domain will be partitioned into finite elements and, in each element, we approximate the solution $\mathbf{u}$ by

$$\mathbf{u} \approx \mathbf{u}_h^e = \sum_{j=1}^{n_{\text{dof}}^e} \psi_j [\, u_1, \ \ldots, u_{n_{\text{nodes}}}, \quad a_1, \ \ldots, a_{n_a}, \quad b_1, \ \ldots, b_{n_a}\,]^T \tag{35}$$

where ψ_j are the higher-order hierarchal shape functions [25]. For the p-element solutions presented next, we employ Szabo and Babuška's quadrilateral shape function expansion basis [26], a serendipity expansion built of kernel functions constructed from Legendre polynomials. The element degrees of freedom, $n_{\text{dof}}^e = n_{\text{nodes}} + n_a + n_b$, consist of the element nodal values, $u_1, \ \ldots, u_{n_{\text{nodes}}}$, the edge coefficients, $a_1, \ \ldots, a_{n_a}$, and the interior (bubble) mode coefficients, $b_1, \ \ldots, b_{n_a}$.

Substituting Eq. (35) into Eqs. (33) and (34) yields n_{dof}^e algebraic equations

$$[\mathbf{K}^e + \alpha_\Gamma \mathbf{K}_\Gamma^e]\mathbf{u} = \mathbf{F}^e + \alpha_\Gamma \mathbf{G}^e \tag{36}$$

The element stiffness matrices and equivalent force vectors are defined by

$$\mathbf{K}^e = \int_{\Omega^e} (\mathbf{A}\psi_1, \ldots, \mathbf{A}\psi_{n_{\text{dof}}^e})^T (\mathbf{A}\psi_1, \ldots, \mathbf{A}\psi_{n_{\text{dof}}^e})\, \mathrm{d}\Omega \tag{37}$$

$$\mathbf{F}^e = \int_{\Omega^e} (\mathbf{A}\psi_1, \ldots, \mathbf{A}\psi_{n_{\text{dof}}^e})^T \mathbf{f}\, \mathrm{d}\Omega \tag{38}$$

$$\mathbf{K}_\Gamma^e = \int_{\Gamma^e} (\mathbf{B}\psi_1, \ldots, \mathbf{B}\psi_{n_{\text{dof}}^e})^T (\mathbf{B}\psi_1, \ldots, \mathbf{B}\psi_{n_{\text{dof}}^e})\, \mathrm{d}\Gamma \tag{39}$$

$$\mathbf{G}^e = \int_{\Gamma^e} (\mathbf{B}\psi_1, \ldots, \mathbf{B}\psi_{n_{\text{dof}}^e})^T \mathbf{g}\, \mathrm{d}\Gamma \tag{40}$$

The element stiffness and load vectors are assembled into a global system of equations, which has the form

$$[\mathbf{K} + \alpha_\Gamma \mathbf{K}_\Gamma]\mathbf{u} = \mathbf{F} + \alpha_\Gamma \mathbf{G} \tag{41}$$

For plane elasticity, we adopt a mixed stress-displacement LS model that employs the minimum number of degrees of freedom (five) to formulate a first-order approximation for the two-dimensional elasticity equations. The five degrees of freedom are the three components of the stress tensor σ_{ij} and the two components of the displacement vector, u and v, so that $\mathbf{u} = [\,u \quad v \quad \sigma_{xx} \quad \sigma_{yy} \quad \sigma_{xy}\,]^T$. Note that other definitions for $\mathbf{u}$ are possible. For example, on a boundary, the normal-tangential coordinate system is preferred to the Cartesian system. The two stress equilibrium equations and the three strain-displacement relations, after eliminating strain via constitutive equations, constitute the five governing equations. The first-order system in matrix operator form can be expressed as

$$A_0\mathbf{u} + A_1\mathbf{u}_{,x} + A_2\mathbf{u}_{,y} = \mathbf{f} \tag{42}$$

where

$$A_0 = \begin{bmatrix} 0 & 0 & 1 & 0 & 0 \\ 0 & 0 & 0 & 1 & 0 \\ 0 & 0 & 0 & 0 & 1 \\ 0 & 0 & 0 & 0 & 0 \\ 0 & 0 & 0 & 0 & 0 \end{bmatrix}, \quad A_1 = \begin{bmatrix} \frac{-E}{1-\nu^2} & 0 & 0 & 0 & 0 \\ \frac{-\nu E}{1-\nu^2} & 0 & 0 & 0 & 0 \\ 0 & \frac{-E}{2(1+\nu)} & 0 & 0 & 0 \\ 0 & 0 & 1 & 0 & 0 \\ 0 & 0 & 0 & 0 & 1 \end{bmatrix}$$

$$A_2 = \begin{bmatrix} 0 & \frac{-\nu E}{1-\nu^2} & 0 & 0 & 0 \\ 0 & \frac{-E}{1-\nu^2} & 0 & 0 & 0 \\ \frac{-E}{2(1+\nu)} & 0 & 0 & 0 & 0 \\ 0 & 0 & 0 & 0 & 1 \\ 0 & 0 & 0 & 1 & 0 \end{bmatrix}, \quad \mathbf{f} = \begin{bmatrix} 0 \\ 0 \\ 0 \\ -f_x \\ -f_y \end{bmatrix} \tag{43}$$

The characteristic polynomial associated with Eqs. (42) and (43) is $\det(A_1\xi + A_2\eta) = 0$. For an elliptic system, all nonzero roots of the characteristic equation are complex. Since complex roots appear as pairs of complex conjugates, a system with an odd number of variables cannot be strictly elliptic. Thus, even though the physics of elasticity systems are elliptic in nature, the first-order formulation given by Eq. (43) is not numerically elliptic. However, Eq. (43) represents the minimum number of degrees of freedom required to formulate an element approximation for a first-order plane elasticity formulation. Several numerical results indicate that, although the system is no longer elliptic for these formulations, the theoretical elliptic convergence rates may still be achieved when compared with an elliptic formulation with an equivalent number of degrees of freedom [27]. Although LSFEM is not theoretically constrained by the stability problems associated with the mixed weak-form Galerkin finite element model [28], a growing consensus is that LSFEM mixed (stress displacement) formulation for elasticity can still be beset by problems of slow convergence for low polynomial orders (e.g., $p < 4$) [18,29–31]. This is readily overcome by employing slightly higher-order polynomial shape functions, which also theoretically improves the convergence rate on an optimally graded mesh. Mixed formulations are also attractive compared with strict displacement formulation elements, since they allow direct access to the stress variables for application of traction boundary conditions and the calculation of stress sensitivities.

V. Plate with a Hole

The first-order LS continuous sensitivity method is demonstrated by two example problems based on the classic plate with a hole problem (Fig. 4). The first example is an infinite plate with a circular hole subject to uniaxial tension for which an analytic solution exists [26]. The analytic elasticity solution permits an analytic sensitivity solution that is convenient to validate the CSE solution and may prove useful as a closed-form validation for other plane elasticity CSE formulations. The second example is a shape optimization problem for a biaxially loaded finite plate. We first present details of the LS-CSE solution to an infinite plate for which an analytic solution exists, and then we use the CSE solution to optimize the problem considered in [8]. The objective of these two examples is to provide sufficient detail in the derivation and results such that this problem can serve as a verification benchmark for structural sensitivity analysis.

Determining the stress concentration for a thin plate with an unstressed hole is a classic problem in the strength of materials and a common exercise in FEM analysis. An analytic solution exists for a circular hole in an infinite plate subject to uniaxial tension [26], and results for finite plates under biaxial loading with a variety of hole dimensions are plotted as a function of load and plate/hole dimensions [32,33]. To illustrate the LS continuous sensitivity method, we consider the shape optimization of an elliptic cutout in a biaxially loaded plate (Fig. 4). The objective of the optimization is to obtain a uniform distribution of tangential stress along the hole. The problem was posed and solved by Bhaskaran and Berkooz [8] using a sensitivity equation method, but details of the sensitivity calculations were not included in the paper.

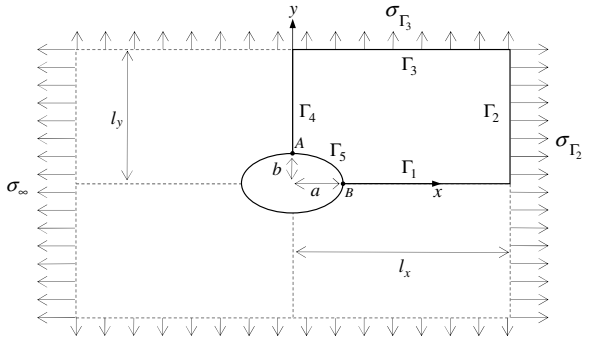

Fig. 4 Plate with an elliptical hole.

For the first example, consider an infinite plate with a circular hole, $a = b = \frac{1}{4}$ subject to a uniaxial load in the x direction, $\sigma_{\Gamma_2} = \sigma_\infty = 10$. By virtue of biaxial symmetry, only a quadrant of the domain is needed for the computational domain (boundary conditions are given in Table 2). To obtain LSFEM results that can be compared with the analytic solution, the analytic normal and tangential stress distribution on boundaries Γ_2 and Γ_3 are imposed as boundary conditions (take $l_x = l_y = 4a = 1$). The analytic displacement and stress solutions for a circular hole are [26]

$$u(r,\theta) = \frac{\sigma_\infty a}{8G}\left\{\frac{r}{a}(\kappa+1)\cos\theta + 2\frac{a}{r}[(1+\kappa)\cos\theta + \cos 3\theta] - 2\frac{a^3}{r^3}\cos 3\theta\right\} \tag{44}$$

$$v(r,\theta) = \frac{\sigma_\infty a}{8G}\left\{\frac{r}{a}(\kappa-3)\sin\theta + 2\frac{a}{r}[(1-\kappa)\sin\theta + \sin 3\theta] - 2\frac{a^3}{r^3}\sin 3\theta\right\} \tag{45}$$

$$\sigma_{xx}(r,\theta) = \sigma_\infty\left[1 - \frac{a^2}{r^2}\left(\frac{3}{2}\cos 2\theta + \cos 4\theta\right) + \frac{3}{2}\frac{a^4}{r^4}\cos 4\theta\right] \tag{46}$$

$$\sigma_{yy}(r,\theta) = \sigma_\infty\left[-\frac{a^2}{r^2}\left(\frac{1}{2}\cos 2\theta - \cos 4\theta\right) - \frac{3}{2}\frac{a^4}{r^4}\cos 4\theta\right] \tag{47}$$

$$\sigma_{xy}(r,\theta) = \sigma_\infty\left[-\frac{a^2}{r^2}\left(\frac{1}{2}\sin 2\theta + \sin 4\theta\right) + \frac{3}{2}\frac{a^4}{r^4}\sin 4\theta\right] \tag{48}$$

where $\kappa = (3-\nu)/(1+\nu)$ and the modulus of rigidity, $G = E/[2(1+\nu)]$. We take Poisson's ratio, $\nu = \frac{1}{3}$, and nondimensionalize the equations so that $E = 1$. Analytic sensitivities for the hole radius are readily obtained by differentiating Eqs. (44–48) with respect to a. The analytic sensitivities are

Table 2 Boundary conditions for plate with a circular hole

Boundary	Boundary condition
Γ_1	$v = 0$, $\sigma_{xy} = 0$ plate symmetry
Γ_2	σ_{xx} and σ_{xy} analytic solution
Γ_3	σ_{yy} and σ_{xy} analytic solution
Γ_4	$u = 0$, $\sigma_{xy} = 0$ plate symmetry
Γ_5	$\sigma_n = 0$, $\sigma_\tau = 0$ stress free hole

$$u_{,a} = \frac{\sigma_\infty}{8G}\left\{4\frac{a}{r}[(1+\kappa)\cos\theta + \cos 3\theta] - 8\frac{a^3}{r^3}\cos 3\theta\right\} \quad (49)$$

$$v_{,a} = \frac{\sigma_\infty}{8G}\left[4\frac{a}{r}[(1-\kappa)\sin\theta + \sin 3\theta] - 8\frac{a^3}{r^3}\sin 3\theta\right] \quad (50)$$

$$\sigma_{xx,a} = \sigma_\infty\left[-\frac{a}{r^2}(3\cos 2\theta + 2\cos 4\theta) + 6\frac{a^3}{r^4}\cos 4\theta\right] \quad (51)$$

$$\sigma_{yy,a} = \sigma_\infty\left[-\frac{a}{r^2}(\cos 2\theta - 2\cos 4\theta) - 6\frac{a^3}{r^4}\cos 4\theta\right] \quad (52)$$

$$\sigma_{xy,a} = \sigma_\infty\left[-\frac{a}{r^2}(\sin 2\theta + 2\sin 4\theta) + 6\frac{a^3}{r^4}\sin 4\theta\right] \quad (53)$$

The LSFEM solution for an 18-element mesh with eighth-order polynomials ($p = 8$) is given in Fig. 5. The 18-element mesh is a convenient, moderately coarse mesh that demonstrates the value of the high-order p elements used in the solution. Convergence studies (h refinement vs p refinement) were accomplished but are not included in this paper since they did not contribute the to primary interest of sensitivity analysis. The solution along the hole, Γ_5, is compared with the analytic solution in Fig. 6. One of the advantages of an LSFEM approach is that the solution permits a readily available error estimate in the form of the residual Eq. (31). Both the residual and the error norm are on the order of 10^{-4} for this relatively coarse mesh and moderate p value. The peak normal stress at the apex of the hole is 30 leading to a stress-concentration factor of three, which matches the result obtained from strength of materials [32].

Since the elasticity equations are linear, the LS-CSE first-order matrix operators are identical to the elasticity system operators in Eq. (43). The boundary conditions at the hole remain the same (stress free) regardless of hole radius; thus, the total material derivative of radial and shear along the hole is zero. Therefore, the CSE boundary conditions along the hole are determined only by the convection term in Eq. (15). Taking the hole radius a as the shape parameter, the Γ_1, Γ_4, and Γ_5 boundaries change with the hole. The hole coordinates are easily parameterized in polar coordinates as

$$X_{\Gamma_5} = \{(\,a \quad \theta\,)^T\}_{(r\theta)} \quad (54)$$

so that

$$X_{\Gamma_5,a} = \{(\,1 \quad 0\,)^T\}_{(r\theta)} \quad (55)$$

Similarly, in Cartesian coordinates,

$$X_{\Gamma_1} = \left\{\left(\lfloor 1-\xi \quad \xi \rfloor \begin{Bmatrix} a \\ 1 \end{Bmatrix} \quad 0\right)^T \middle| \xi \in [0,1]\right\}_{(xy)} \quad (56)$$

$$X_{\Gamma_4} = \left\{\left(0 \quad \lfloor 1-\xi \quad \xi \rfloor \begin{Bmatrix} b \\ 1 \end{Bmatrix}\right)^T \middle| \xi \in [0,1]\right\}_{(xy)} \quad (57)$$

Then, for a circular hole with $a = b$,

$$X_{\Gamma_1,a} = \{(\,1-\xi \quad 0\,)^T | \xi \in [0,1]\}_{(xy)} \quad (58)$$

$$X_{\Gamma_4,a} = \{(\,0 \quad 1-\xi\,)^T | \xi \in [0,1]\}_{(xy)} \quad (59)$$

Now, differentiating the boundary conditions along Γ_1 and Γ_4 and evaluating the convection term with Eqs. (58) and (59) yields the CSE boundary conditions for the Γ_1 and Γ_4 boundaries:

$$\begin{Bmatrix} {}^a v(\xi) \\ {}^a\sigma_{xy}(\xi) \end{Bmatrix}_{\Gamma_1} = \frac{\mathrm{D}\{\,v \quad \sigma_{xy}\,\}_{\Gamma_1}^T}{\mathrm{D}a} - \begin{Bmatrix} \nabla v \\ \nabla\sigma_{xy} \end{Bmatrix} \cdot \frac{\partial X_{\Gamma_1}}{\partial a} = 0$$
$$- \begin{Bmatrix} (1-\xi)v_{,x} \\ (1-\xi)\sigma_{xy,x} \end{Bmatrix}_{\xi\in[0,1]} = 0 \quad (60)$$

$$\begin{Bmatrix} {}^a u(\xi) \\ {}^a\sigma_{xy}(\xi) \end{Bmatrix}_{\Gamma_4} = \frac{\mathrm{D}\{\,u \quad \sigma_{xy}\,\}_{\Gamma_4}^T}{\mathrm{D}a} - \begin{Bmatrix} \nabla u \\ \nabla\sigma_{xy} \end{Bmatrix} \cdot \frac{\partial X_{\Gamma_4}}{\partial a} = 0$$
$$- \begin{Bmatrix} (1-\xi)u_{,y} \\ (1-\xi)\sigma_{xy,y} \end{Bmatrix}_{\xi\in[0,1]} = 0 \quad (61)$$

For Γ_5, the gradients in the convection term must be calculated from the gradients of the LSFEM solution and are not available by inspection as they are for Γ_1 and Γ_4. The Γ_5 CSE boundary conditions are

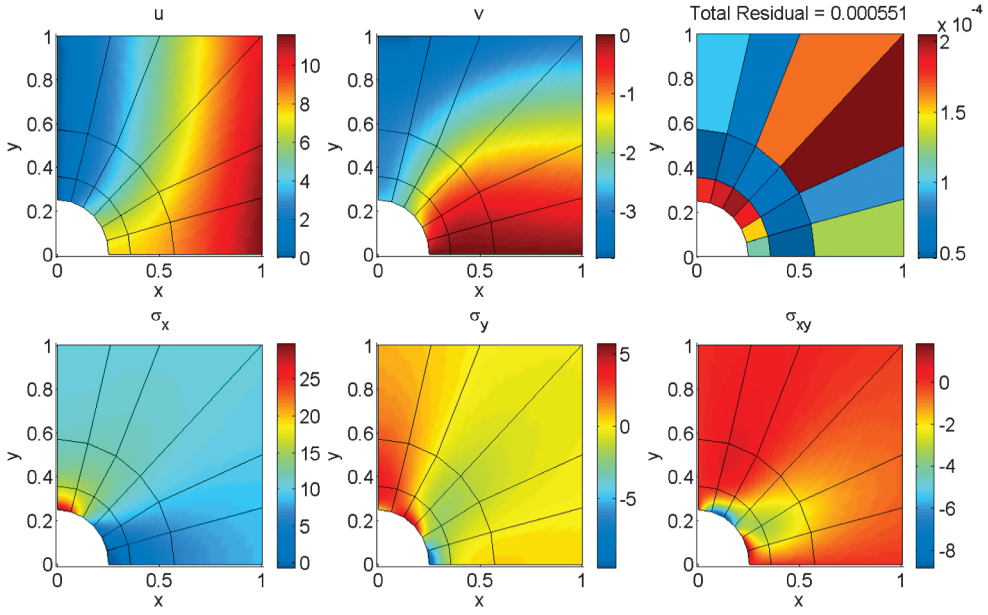

Fig. 5 LSFEM solution ($p = 8$) for displacements (u, v), stresses (σ_x, σ_y, σ_{xy}), and residual error norm of a quarter plate with a circular hole subject to a normal-x stress value of 10.

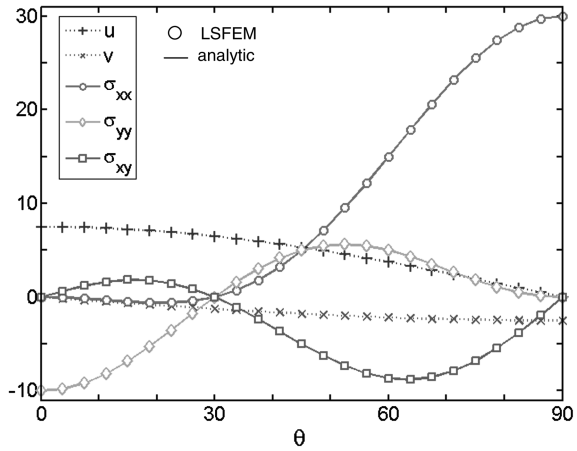

Fig. 6 Comparison of LSFEM and analytic solution along the hole ($p = 8$).

$$\begin{Bmatrix} {}^a\sigma_{rr} \\ {}^a\sigma_{r\theta} \end{Bmatrix}_{\Gamma_5} = \frac{\mathrm{D}\{\,\sigma_{rr} \quad \sigma_{r\theta}\,\}_{\Gamma_5}^{T}}{\mathrm{D}a} - \nabla_{(r\theta)} \begin{Bmatrix} \sigma_{rr} \\ \sigma_{r\theta} \end{Bmatrix} \cdot \frac{\partial}{\partial a}\{X_{\Gamma_5}\}_{(r\theta)} = \begin{Bmatrix} -\sigma_{rr,r} \\ -\sigma_{r\theta,r} \end{Bmatrix} \tag{62}$$

where it should be noted that the gradient operator and boundary set definition must be expressed in the same coordinate system. The radial, shear, and tangential stress components along the hole are given by

$$\begin{bmatrix} \sigma_{rr} & \sigma_{r\theta} \\ \sigma_{\theta r} & \sigma_{\theta\theta} \end{bmatrix} = \begin{bmatrix} \cos\theta & \sin\theta \\ -\sin\theta & \cos\theta \end{bmatrix} \begin{bmatrix} \sigma_{xx} & \sigma_{xy} \\ \sigma_{yx} & \sigma_{yy} \end{bmatrix} \begin{bmatrix} \cos\theta & -\sin\theta \\ \sin\theta & \cos\theta \end{bmatrix} \tag{63}$$

Using this coordinate transformation and the polar coordinate gradient operator

$$\nabla_{(r\theta)} \equiv \left\langle \frac{\partial}{\partial r} \quad \frac{1}{r}\frac{\partial}{\partial \theta} \right\rangle \tag{64}$$

the radial gradients of the normal and shear stress components are

$$\sigma_{rr,r} = \sigma_{xx,r}\cos^2(\theta) + \sigma_{yy,r}\sin^2(\theta) + 2\sigma_{xy,r}\sin(\theta)\cos(\theta) \tag{65}$$

$$\sigma_{r\theta,r} = -(\sigma_{xx,r} - \sigma_{yy,r})\sin\theta\cos\theta + \sigma_{xy,r}(\cos^2\theta - \sin^2\theta) \tag{66}$$

Expressing the radial gradient through the chain rule

$$\frac{\mathrm{d}}{\mathrm{d}r}(\cdot) = \frac{\partial(\cdot)}{\partial x}\frac{\partial x}{\partial r} + \frac{\partial(\cdot)}{\partial y}\frac{\partial y}{\partial r}$$

and noting that $x_{,r} = \cos\theta$ and $y_{,r} = \sin\theta$ yields the final radial and tangential stress CSE boundary conditions in terms of Cartesian components,

$$\begin{aligned} {}^a\sigma_{rr} = -\sigma_{rr,r} = &-(\sigma_{xx,x}\cos\theta + \sigma_{xx,y}\sin\theta)\cos^2\theta \\ &- (\sigma_{yy,x}\cos\theta + \sigma_{yy,y}\sin\theta)\sin^2\theta + \cdots \\ &- 2(\sigma_{xy,x}\cos\theta + \sigma_{xy,y}\sin\theta)\cos\theta\sin\theta \end{aligned} \tag{67}$$

$$\begin{aligned} {}^a\sigma_{r\theta} = -\sigma_{r\theta,r} = &[(\sigma_{xx,x} - \sigma_{yy,x})\cos\theta \\ &+ (\sigma_{xx,y} - \sigma_{yy,y})\sin\theta]\cos\theta\sin\theta + \cdots \\ &- (\sigma_{xy,x}\cos\theta + \sigma_{xy,y}\sin\theta)(\cos^2\theta - \sin^2\theta) \end{aligned} \tag{68}$$

The spatial derivatives of the Cartesian stress components required in Eqs. (67) and (68) come from the gradients of the shape functions of the LSFEM solution. The analytic and LSFEM-derived boundary conditions for the hole in the CSE problem are compared in Fig. 7. Note that, by using higher-order p elements, the sensitivity boundary condition accuracy can be improved by increasing the p value used for underlying elasticity problem.

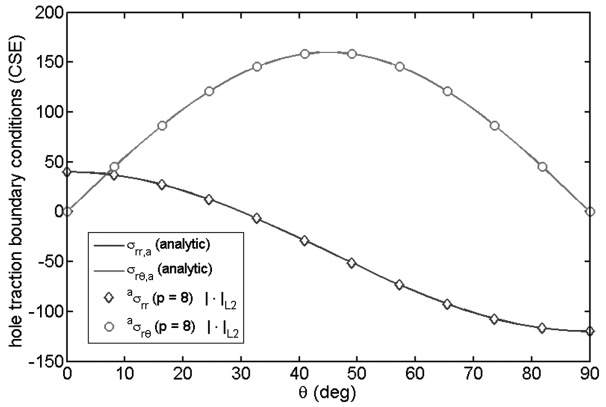

Fig. 7 Comparison of analytic and LSFEM-derived sensitivity boundary conditions.

The LS-CSE solution for the same 18-element mesh ($p = 8$) is given in Fig. 8. The local sensitivity solution for tangential stress along the hole is compared with the analytic solution in Fig. 9. The finite difference sensitivity and the total sensitivity calculated from the LS-CSE solution are also plotted in Fig. 9. The tangential stress along the hole of an infinite plate does not depend on the hole radius, so the total sensitivity of the tangential stress at material points on the hole boundary is zero, as expected.

Figure 10 plots the p convergence for both the elasticity and sensitivity problems as well as the convergence of the maximum stress within the plate normalized by the loading stress. Note that the stress concentration asymptotically approaches the theoretical stress-concentration factor of three. The residual and the error norm for the $p = 8$ sensitivity solution given in Figs. 8 and 9 are both on the order of 10^{-2}; two orders of magnitude greater than the original LSFEM problem at the same p value. A polynomial order of 11 yields the equivalent 10^{-4} error for the LS-CSE problem, as compared with the original LSFEM residual at $p = 8$. CSE systems typically have steeper gradients in the vicinity of a boundary subject to shape variation than the original problem and often require a higher p value (or finer mesh) than the original system, a result previously observed [10,34]. It is convenient to use the same mesh for both the original system and the sensitivity system and to obtain the more refined solution through higher-order p elements. This is a distinct advantage of higher-order FEM, since p refinement allows a straightforward means to achieve a refined solution without needing a refined mesh.

VI. Shape Optimization of a Biaxially Loaded Plate with a Hole

Bhaskaran and Berkooz [8] posed a shape optimization problem based on the plate with a hole, which seeks the optimum dimensions of an elliptical hole to obtain a uniform distribution of the tangential stress along the hole. Banichuk [35] previously offered an elegant proof that the shape that minimizes the stress in the infinite plate is an ellipse, but the current interest is in the application of CSE to solve the finite plate shape optimization problem. The semimajor axis of the ellipse is constrained to be one fifth of the edge of the square plate, and the semiminor axis is taken as the design parameter. The applied loads are $\sigma_{xx} = 1$ MPa and $\sigma_{yy} = 0.75$ MPa. The objective function to be minimized is

$$J = \int_{\Gamma_5} (\sigma_{\theta\theta} - \bar{\sigma}_{\theta\theta})^2 \,\mathrm{d}E \tag{69}$$

where E is the eccentric anomaly of the elliptical hole and the mean tangential stress along the hole is

$$\bar{\sigma}_{\theta\theta} = \frac{2}{\pi}\int_0^{\pi/2} \sigma_{\theta\theta} \,\mathrm{d}E \tag{70}$$

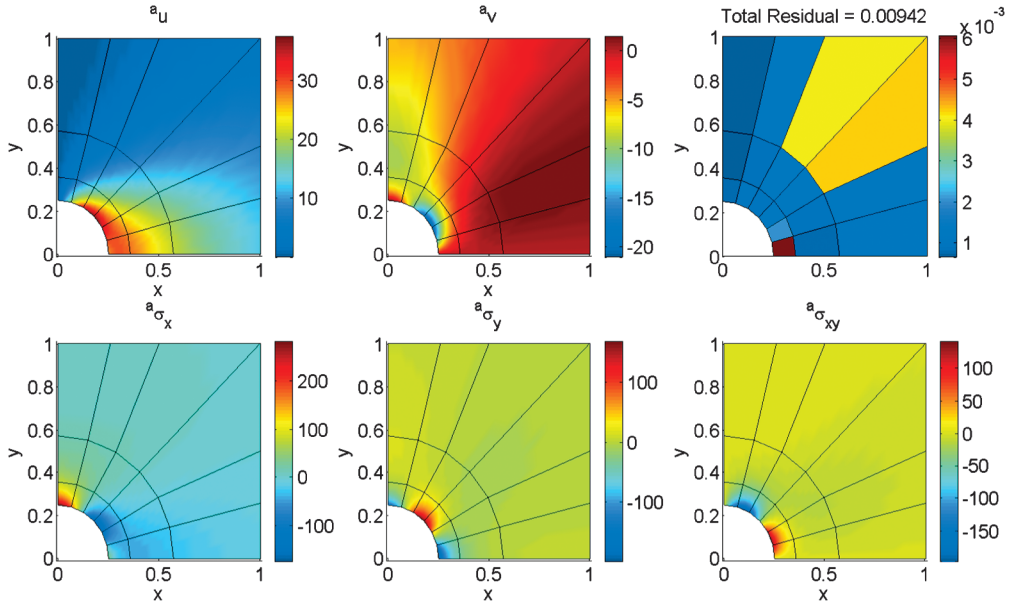

Fig. 8 LS-CSE solution ($p = 8$) and residual error norm for the sensitivity of field variables to hole radius a for a quarter plate with a circular hole.

Bhaskaran and Berkooz [8] posed the objective function as an integral over arc length. Evaluating the objective function in Eq. (69) with respect to eccentric anomaly instead of arc length is equivalent to Bhaskaran and Berkooz [8] but is simpler to implement, since the sensitivity of the arc length (which is a function of semiminor axis of the ellipse) does not have to be calculated. The only boundaries defined in Fig. 4 that depend on the semiminor axis are Γ_4 and Γ_5. The first is parameterized by Eq. (57), and Γ_5 is given (in Cartesian coordinates) by

$$X_{\Gamma_5} = \{(a\cos E \quad b\sin E)^T\} \tag{71}$$

so that

$$X_{\Gamma_5,b} = \{(0 \quad \sin E)^T\} \tag{72}$$

The objective functional material derivative with respect to the semiminor axis is

$$\mathrm{D}_b J = 2\int_{\Gamma_5} (\sigma_{\theta\theta} - \bar{\sigma}_{\theta\theta})(\mathrm{D}_b\sigma_{\theta\theta} - \mathrm{D}_b\bar{\sigma}_{\theta\theta})\,\mathrm{d}E \tag{73}$$

where, for the parameterization given by Eq. (71),

$$\mathrm{D}_b\sigma_{\theta\theta} = {}^b\sigma_{\theta\theta} + \sin E\sigma_{\theta\theta,y} \tag{74}$$

$$\mathrm{D}_b\bar{\sigma}_{\theta\theta} = \frac{2}{\pi}\int_0^{\pi/2} {}^b\sigma_{\theta\theta}\,\mathrm{d}E + \frac{2}{\pi}\int_0^{\pi/2} \sin E\sigma_{\theta\theta,y}\,\mathrm{d}E \tag{75}$$

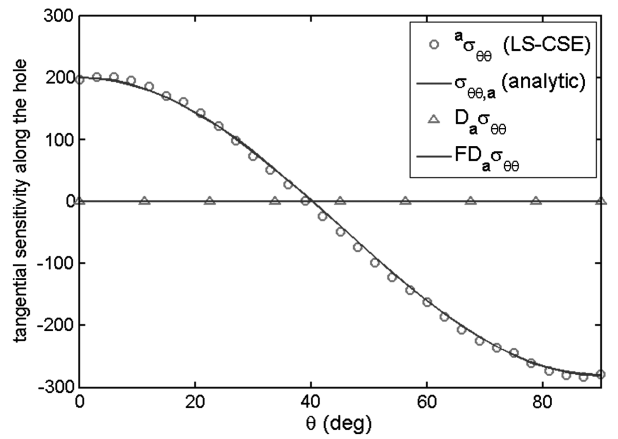

Fig. 9 Comparison of analytic, finite difference, and LS-CSE solutions along the hole boundary for tangential stress sensitivity to hole radius a.

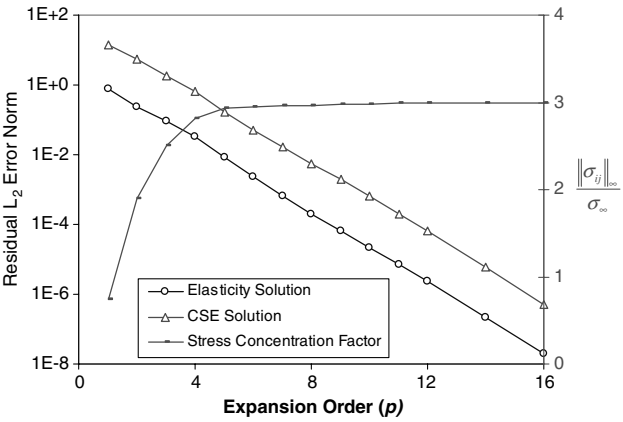

Fig. 10 Elasticity and sensitivity problem p convergence and stress-concentration convergence for a uniaxially loaded plate with a circular hole.

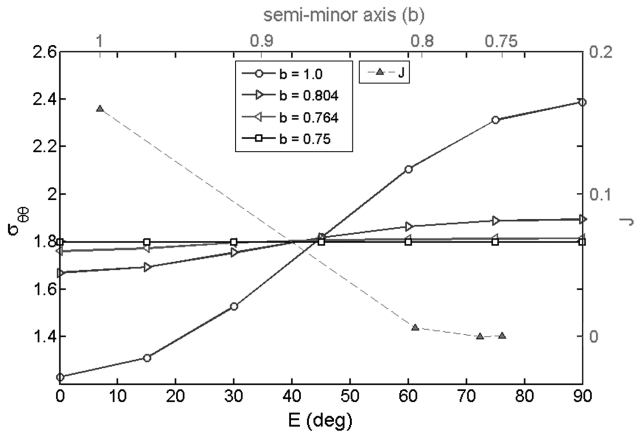

Fig. 11 Tangential stress optimization convergence to uniform value ($\bar{\sigma}_{\theta\theta} = 1.797$) as a function of eccentric anomaly (E) and objective function value as a function of semiminor axis (b).

Table 3 Plate with an elliptical hole optimization

b	J	D_bJ	$\bar{\sigma}_{\theta\theta}$
1.0	1.56E − 1	1.960	1.814
0.804	6.00E − 3	0.363	1.799
0.764	2.88E − 4	0.140	1.797
0.75	9.22E − 5	−0.0118	1.797

The tangential stress sensitivity ${}^b\sigma_{\theta\theta}$ is determined from the solution to the LS-CSE system. The CSE problem has homogenous boundary conditions on every boundary, except Γ_5, which are given by

$$\begin{Bmatrix} {}^b\sigma_{rr} \\ {}^b\sigma_{r\theta} \end{Bmatrix} = 0 - \nabla \begin{Bmatrix} \sigma_{rr} \\ \sigma_{r\theta} \end{Bmatrix} \cdot \begin{Bmatrix} 0 \\ \sin E \end{Bmatrix} = \begin{Bmatrix} -\sigma_{rr,y} \sin E \\ -\sigma_{r\theta,y} \sin E \end{Bmatrix} \tag{76}$$

The analytic stress-concentration factors for an infinite biaxially loaded plate are based on the maximum normal stresses σ_A and σ_B [32]:

$$K_{tA} \equiv \frac{\sigma_A}{\sigma_{\Gamma_2}} = \frac{\sigma_{\Gamma_3}}{\sigma_{\Gamma_2}} \left[1 + \frac{2}{b/a} \right] - 1 \tag{77}$$

$$K_{tB} \equiv \frac{\sigma_B}{\sigma_{\Gamma_2}} = 1 + \frac{2b}{a} - \frac{\sigma_{\Gamma_3}}{\sigma_{\Gamma_2}} \tag{78}$$

where the points A and B are the apex and shoulder points indicated in Fig. 4. Equating the stress concentration at these two points yields the desired uniform tangential stress around the ellipse and requires that

$$\frac{b}{a} = \frac{\sigma_{\Gamma_3}}{\sigma_{\Gamma_2}} \tag{79}$$

which yields an optimum semiminor axis of 0.75 for the given loading. For an infinite plate, this yields a uniform stress-concentration value of 1.75 around the hole. Various finite width corrections [32] for semi-infinite plates under uniaxial loading yield approximate values 3% higher for stress concentrations for hole-to-edge ratios of 0.2. This implies a uniform tangential stress of 1.8 MPa for the present case, which is very close to the 1.797 MPa result obtained from the simple line-search optimization based on the LS-CSE objective gradient of Eq. (73). The convergence history for the tangential stress is plotted in Fig. 11 along with values of the objective function as a function of the eccentric anomaly along the hole. Values of the objective function and the total objective function gradient are also summarized in Table 3. Note also that the residual error of 10^{-3} is comparable to the accuracy obtained in achieving a uniform stress distribution. This highlights that advantage of the built-in error estimate of the LSFEM approach.

VII. Conclusions

A LS formulation for solving the first-order CSEs for shape design optimization problems was developed. Because of commutativity of the local derivative and the simpler sensitivity boundary conditions, it is generally more convenient to pose and solve the local form of the sensitivity equations for shape variation problems, but the solution depends on the boundary parameterization and is not unique. However, it is straightforward to convert the local CSE solution to a total derivative solution. Optimization is typically performed with respect to material coordinates, particularly for structural elasticity problems, thus the total derivative sensitivity is generally desired. Although the local CSE solution is not unique, the total sensitivity, which is given at material coordinates, is unique. The advantage of expressing the CSE system in local-derivative form is that only the boundary parameterization needs be described, which avoids having to define a parameterization or transformation function for the entire domain. The boundary parameterization method adopted here is also simpler than some previous results that appear in the literature, because the sensitivity is only needed on the boundary to define the continuous sensitivity boundary-value problem. Moreover, the choice of boundary coordinate adopted here simplified the stress sensitivity boundary conditions such that they were expressed in terms of the stress vector rather than components of the stress tensor. The first-order formulation of the elasticity and the CSE system also avoids the accuracy problems associated with determining the higher-order derivatives for Neumann-type sensitivity boundary conditions.

In the present work, the continuous sensitivity system was solved using the same high-order LSFEM that was used to solve the underlying elasticity problem. The LSFEM approach is attractive in that it allows a stable first-order form for elasticity, a better approximation of stress gradients compared with the weak-form Galerkin displacement formulations, an inherent error estimate, and flexibility in norm choice. The improved accuracy of the stress gradients inherent in the first-order mixed formulation of the elasticity system is particularly important, since the gradients of the underlying elasticity solution are used to pose the boundary conditions for the sensitivity system. The higher-order p element implementation also permitted a straightforward means to achieve a refined solution without needing a refined mesh. Thus, both the structural and sensitivity systems can be easily solved to any desired level of convergence using a single computational mesh. This is particularly important since, as observed in the literature, the CSE solution often requires different resolution than the original system.

Overall, the LS continuous sensitivity method is a good option for the optimization of structural elasticity problems. There is no need to determine the proper step size as in finite difference methods: a requirement that can become problematic in multivariate optimization problems. Additionally, since the CSEs are always linear, there is a potential computational savings in not having to calculate multiple solutions to the underlying nonlinear system, as is required for finite difference approaches. Furthermore, finite difference methods can only yield the total derivative, whereas the continuous sensitivity method yields both local and total derivatives. The continuous sensitivity approach has the advantage over discrete sensitivity methods of not having to invert the mesh Jacobian for shape variation problems in which the domain (and hence the discrete mesh) is changed. This can also result in significant computational savings for the LS-CSE approach compared with discrete sensitivity methods.

Acknowledgments

The U. S. Air Force Office of Scientific Research (AFOSR) and the U. S. Air Force Research Laboratory (AFRL) Air Vehicles Directorate funded this research. The authors gratefully acknowledge the support of AFOSR program manager Fariba Fahroo and the AFRL Senior Aerospace Engineers Raymond Kolonay, Phillip Beran, and Maxwell Blair. The last author acknowledges support of the research by the Oscar S. Wyatt Endowed Chair.

References

[1] Haug, E. J., Choi, K. K., and Komkov, V., "Design Sensitivity Analysis of Structural Systems," *Mathematics in Science and Engineering*, Vol. 177, Academic Press, Orlando, FL, 1986.

[2] Choi, K. K., and Kim, N. H., "Structural Sensitivity Analysis and Optimization," *Mechanical Engineering Series*, Springer, New York, 2005.

[3] Dems, K., and Haftka, R. T., "Two Approaches to Sensitivity Analysis for Shape Variation Of Structures," *Mechanics Based Design of Structures and Machines*, Vol. 16, No. 4, 1988, pp. 501–522. doi:10.1080/08905458808960274

[4] Haftka, R. T., and Gürdal, Z., "Elements of Structural Optimization," *Solid Mechanics and its Applications*, Vol. 11, Kluwer Academic, Dordrecht, The Netherlands, 1992.

[5] Borggaard, J., and Burns, J., "A PDE Sensitivity Equation Method for Optimal Aerodynamic Design," *Journal of Computational Physics*, Vol. 136, No. 2, 1997, pp. 366–384. doi:10.1006/jcph.1997.5743

[6] Dems, K., and Mroz, Z., "Variational Approach to First- and Second-Order Sensitivity Analysis of Elastic Structures," *International Journal*

for Numerical Methods in Engineering, Vol. 21, No. 4, 1985, pp. 637–661.
doi:10.1002/nme.1620210405

[7] Borggaard, J., and Burns, J., "A Sensitivity Equation Approach to Shape Optimization in Fluid Flows," NASA Langley Research Center, CR 191598, 1994.

[8] Bhaskaran, R., and Berkooz, G., "Optimization of Fluid-Structure Interaction Using the Sensitivity Equation Approach," *Fluid-Structure Interaction, Aeroelasticity, Flow-Induced Vibrations and Noise*, Vol. 53-1, American Society of Mechanical Engineers, Fairfield, NJ, 1997, pp. 49–56.

[9] Turgeon, E., Pelletier, D., and Borggaard, J., "A Continuous Sensitivity Equation Approach to Optimal Design in Mixed Convection," AIAA Paper 1999-3625, 1999.

[10] Stanley, L. G. D., and Stewart, D. L., *Design Sensitivity Analysis: Computational Issues of Sensitivity Equation Methods*, Society for Industrial and Applied Mathematics, Philadelphia, 2002.

[11] Étienne, S., and Pelletier, D., "A General Approach to Sensitivity Analysis of Fluid–Structure Interactions," *Journal of Fluids and Structures*, Vol. 21, No. 2, 2005, pp. 169–186.
doi:10.1016/j.jfluidstructs.2005.07.001

[12] Étienne, S., Hay, A., and Garon, A., "Shape Sensitivity Analysis of Fluid-Structure Interaction Problems," 36th AIAA Fluid Dynamics Conference and Exhibit, AIAA Paper 2006-3217, June 2006.

[13] Étienne, S., Hay, A., and Garon, A., "Sensitivity Analysis of Unsteady Fluid-Structure Interaction Problems," 45th AIAA Aerospace Sciences Meeting and Exhibit, AIAA Paper 2007-0332, 2007.

[14] Jameson, A., "Aerodynamic Optimization via Control Theory," *Journal of Scientific Computing*, Vol. 3, No. 3, 1988, pp. 233–260.
doi:10.1007/BF01061285

[15] Jameson, A., Shankaran, S., and Martinelli, L., "Continuous Adjoint Method for Unstructured Grids," *AIAA Journal*, Vol. 46, No. 5, 2008, pp. 1226–1239.
doi:10.2514/1.25362

[16] Wickert, D. P., "Least-Squares Continuous Sensitivity Analysis for Nonlinear Fluid-Structure Interaction," Ph.D. Dissertation, Air Force Inst. of Technology, Wright-Patterson AFB, OH, Aug. 2009.

[17] Dems, K., and Mroz, Z., "Variational Approach by Means of Adjoint Systems To Structural Optimization and Sensitivity Analysis. I: Variation of Material Parameters Within Fixed Domain," *International Journal of Solids and Structures*, Vol. 19, No. 8, 1983, pp. 677–692.
doi:10.1016/0020-7683(83)90064-1

[18] Pontaza, J. P., and Reddy, J. N., "Mixed Plate Bending Elements Based on Least-Squares Formulation," *International Journal for Numerical Methods in Engineering*, Vol. 60, No. 5, 2004, pp. 891–922.
doi:10.1002/nme.991

[19] Arnold, D. N., and Winther, R., "Mixed Finite Elements for Elasticity," *Numerical Mathematics*, Vol. 92, No. 3, 2002, pp. 401–419.
doi:10.1007/s002110100348

[20] Arnold, D. N., and Winther, R., "Mixed Finite Elements for Elasticity in the Stress-Displacement Formulation," *Contemporary Mathematics*, Vol. 329, 2003, pp. 33–42.

[21] Arnold, D. N., and Awanou, G., "Rectangular Mixed Finite Elements for Elasticity," *Mathematical Models and Methods in Applied Sciences*, Vol. 15, No. 9, 2005, pp. 1417–1429.
doi:10.1142/S0218202505000741

[22] Reddy, J. N., *Applied Functional Analysis and Variational Methods in Engineering*, McGraw–Hill, New York, 1986.

[23] Jiang, B., *The Least-Squares Finite Element Method: Theory and Applications in Computational Fluid Dynamics and Electromagnetics*, Springer, New York, 1998.

[24] Reddy, J. N., *An Introduction to the Finite Element Method*, 3rd ed., McGraw–Hill, New York, 2006.

[25] Šolín, P., Segeth, K., and Doležel, I., *Higher-Order Finite Element Methods*, CRC Press, Boca Raton, FL, 2004.

[26] Szabo, B. A. and Babuška, I., *Finite Element Analysis*, Wiley, New York, 1991.

[27] Rasmussen, C. C., "Nonlinear Transient Gust Response Using a Fully-Coupled Least-Squares Finite Element Formulation for Fluid-Structure Interaction," Ph.D. Dissertation, Air Force Inst. of Technology, Wright-Patterson AFB, OH, Dec. 2008.

[28] Arnold, D. N., "Mixed Finite Element Methods for Elliptic Problems," *Computer Methods in Applied Mechanics and Engineering*, Vol. 82, Nos. 1–3, 1990, pp. 281–300.
doi:10.1016/0045-7825(90)90168-L

[29] Pontaza, J. P. and Reddy, J. N., "Least-Squares Finite Element Formulation for Shear-Deformable Shells," *Computer Methods in Applied Mechanics and Engineering*, Vol. 194, Nos. 21–24, 2005, 2464–2493.
doi:10.1016/j.cma.2004.07.041

[30] Wickert, D. P., Roberts, R. W., and Canfield, R. A., "Least-Squares Continuous Sensitivity Equations for an Infinite Plate With A Hole," 49th AIAA/ASME/ASCE/AHS/ASC Structures, Structural Dynamics, and Materials Conference, AIAA Paper 2008-1797, April 2008.

[31] Rasmussen, C., Canfield, R., and Reddy, J. N., "Nonlinear Transient Gust Response Using a Fully-Coupled Least-Squares Finite Element Formulation," 49th AIAA/ASME/ASCE/AHS/ASC Structures, Structural Dynamics, and Materials Conference, AIAA Paper 2008-1821, April 2008.

[32] Peterson, R. E., *Stress Concentration Factors; Charts and Relations Useful in Making Strength Calculations for Machine Parts and Structural Elements*, Wiley, New York, 1974.

[33] Roark, R. J., Young, W. C., and Budynas, R. G., *Roark's Formulas for Stress and Strain*, McGraw–Hill, New York, 2002.

[34] Wickert, D. P., and Canfield, R. A., "Least-Squares Continuous Sensitivity Analysis of an Example Fluid-Structure Interaction Problem," 49th AIAA/ASME/ASCE/AHS/ASC Structures, Structural Dynamics, and Materials Conference, AIAA Paper 2008-1896, April 2008.

[35] Banichuk, N., *Problems and Methods in Optimal Structural Design*, Plenum, New York, 1983.

A. Messac
Associate Editor